Mean-field dynamical density functional theory

2003 J. Phys.: Condens. Matter 15 L147

(http://iopscience.iop.org/0953-8984/15/6/102)

INSTITUTE OF PHYSICS PUBLISHING JOURNAL OF PHYSICS: CONDENSED MATTER

J. Phys.: Condens. Matter **15** (2003) L147–L154 PII: S0953-8984(03)58754-9

LETTER TO THE EDITOR

Mean-field dynamical density functional theory

J Dzubiella and C N Likos[1]

University Chemical Laboratory, Lensfield Road, Cambridge CB2 1EW, UK

Received 24 January 2003
Published 3 February 2003
Online at stacks.iop.org/JPhysCM/15/L147

Abstract

We examine the out-of-equilibrium dynamical evolution of density profiles of ultrasoft particles under time-varying external confining potentials in three spatial dimensions. The theoretical formalism employed is the dynamical density functional theory (DDFT) of Marini Bettolo Marconi and Tarazona (1999 *J. Chem. Phys.* **110** 8032), supplied by an equilibrium excess free energy functional that is essentially exact. We complement our theoretical analysis by carrying out extensive Brownian dynamics simulations. We find excellent agreement between theory and simulations for the whole time evolution of density profiles, demonstrating thereby the validity of the DDFT when an accurate equilibrium free energy functional is employed.

(Some figures in this article are in colour only in the electronic version)

Density functional theory (DFT) is a very powerful tool for the quantitative description of the equilibrium states of many-body systems under arbitrary external fields. It rests on the exact statement that the Helmholtz free energy of the system, $F[\rho]$, is a unique functional of the inhomogeneous one-particle density $\rho(\boldsymbol{r})$. Moreover, the equilibrium profile $\rho_0(\boldsymbol{r})$ minimizes $F[\rho]$ under the constraint of fixed particle number N [1]. The task is then to approximate the unknown functional $F[\rho]$ from which all equilibrium properties of the system follow. Much more challenging is the problem of studying *out-of-equilibrium dynamics* of many-body systems, for which analogous uniqueness and minimization principles are lacking. In this letter, we present results based on a recently proposed dynamical density functional theory (DDFT) formalism and we demonstrate that the latter is capable of describing out-of-equilibrium diffusive processes in colloidal systems at the Brownian timescale.

We are concerned with the dynamics of typical soft-matter systems, such as suspensions of mesoscopic spheres and polymer chains in a microscopic solvent [2]. The enormous difference in mass of the suspended particles and the solvent molecules implies a corresponding separation in the relaxational timescales of the two. At times of the order of the Fokker–Planck scale, $\tau_{\mathrm{FP}} \sim 10^{-14}$ s, the solvent coordinates are already relaxed to thermal equilibrium. On the

[1] Also at: Institut für Theoretische Physik II, Heinrich-Heine-Universität Düsseldorf, Universitätsstraße 1, D-40225 Düsseldorf, Germany.

0953-8984/03/060147+08$30.00

Brownian diffusive timescale, $\tau_B \sim 10^{-9}$ s, the momentum coordinates of the solute particles relax to equilibrium with the heat bath of the solvent molecules and thus a statistical description involving only the positions of the colloids is feasible [3]. In this regime, the evolution of the coordinates $\{\boldsymbol{r}_1(t), \boldsymbol{r}_2(t), \ldots, \boldsymbol{r}_N(t)\}$ of the N colloidal particles is described by the set of stochastic Langevin equations

$$\frac{\mathrm{d}\boldsymbol{r}_i(t)}{\mathrm{d}t} = -\Gamma\nabla_{\boldsymbol{r}_i}\left[\sum_{j\neq i} V(|\boldsymbol{r}_i - \boldsymbol{r}_j|) + V_{\mathrm{ext}}(\boldsymbol{r}_i, t)\right] + \boldsymbol{w}_i(t). \tag{1}$$

In equation (1) above, $V(|\boldsymbol{r}_i - \boldsymbol{r}_j|)$ is the pair (effective) interaction potential between the mesoscopic particles [2], $V_{\mathrm{ext}}(\boldsymbol{r}_i, t)$ is the externally acting potential and $\boldsymbol{w}_i(t) = [w_i^x(t), w_i^y(t), w_i^z(t)]$ is a stochastic term representing the random collisions with the solvent molecules and having the properties

$$\langle w_i^\alpha(t)\rangle = 0 \qquad \text{and} \qquad \langle w_i^\alpha(t) w_j^\beta(t')\rangle = 2D\delta_{ij}\delta_{\alpha\beta}\delta(t-t'), \tag{2}$$

where the averages $\langle\cdots\rangle$ are over the Gaussian noise distribution and $\alpha, \beta = x, y, z$, the Cartesian components. The constants Γ and D stand for the mobility and diffusion coefficients of the particles, respectively, and the Einstein relation gives $\Gamma/D = (k_BT)^{-1} \equiv \beta$. Applying the rules of the Itô stochastic calculus, Marini Bettolo Marconi and Tarazona [4, 5] recast the above equations into the form

$$\Gamma^{-1}\frac{\partial\rho(\boldsymbol{r},t)}{\partial t} = \nabla_r[k_BT\,\nabla_r\rho(\boldsymbol{r},t) + \rho(\boldsymbol{r},t)\,\nabla_r V_{\mathrm{ext}}(\boldsymbol{r},t)] + \nabla_r\left[\int \mathrm{d}^3r'\,\langle\hat\rho(\boldsymbol{r},t)\hat\rho(\boldsymbol{r}',t)\rangle\,\nabla_r V(\boldsymbol{r}-\boldsymbol{r}')\right]. \tag{3}$$

Here, $\hat\rho(\boldsymbol{r},t) = \sum_i \delta(\boldsymbol{r}_i(t) - \boldsymbol{r})$ is the usual one-particle density operator and $\rho(\boldsymbol{r},t) = \langle\hat\rho(\boldsymbol{r},t)\rangle$ is the noise average of this quantity. Up to this point, all is exact. Now, the following *physical assumption* (A) is introduced: as the system follows its relaxation dynamics, the instantaneous two-particle correlations can be approximated by those of a system in thermodynamic equilibrium with a *static* one-particle density $\rho(\boldsymbol{r})$ that is the same as the noise-averaged dynamical one-particle density $\rho(\boldsymbol{r},t)$. Then, equation (3) can be cast into a form involving exclusively the equilibrium density functional $F[\rho]$ as [4, 5]

$$\Gamma^{-1}\frac{\partial\rho(\boldsymbol{r},t)}{\partial t} = \nabla_r\cdot\left[\rho(\boldsymbol{r},t)\,\nabla_r\frac{\delta F[\rho(\boldsymbol{r},t)]}{\delta\rho(\boldsymbol{r},t)}\right], \tag{4}$$

with the free energy functional

$$F[\rho] = k_BT\int \mathrm{d}^3r\,\rho(\boldsymbol{r})\{\ln[\rho(\boldsymbol{r})\Lambda^3] - 1\} + F_{\mathrm{ex}}[\rho] + \int \mathrm{d}^3r\,V_{\mathrm{ext}}(\boldsymbol{r},t)\,\rho(\boldsymbol{r}). \tag{5}$$

The dynamical equation of motion (4) was in fact first derived in a phenomenological way by Dietrich *et al* [6]. In carrying out concrete calculations with the theory put forward above and in comparing them with Brownian dynamics (BD) simulation results based on the microscopic equations of motion, equation (1), two sources of possible discrepancies exist: first, the fundamental assumption (A); and second, the approximate nature of the equilibrium density functional $F_{\mathrm{ex}}[\rho]$ of equation (5). In this work we focus our attention on *ultrasoft particles* for which a very accurate and simple functional $F[\rho]$ is known, namely the *mean-field* or *random-phase approximation* (RPA) functional given by equation (6) below. This guarantees that one can explore the accuracy of the fundamental assumption (A) under well-defined external conditions.

Consider a one-component system of ultrasoft particles. It has been demonstrated that for such systems the following RPA functional is quasi-exact [7–13]:

$$F_{\mathrm{ex}}[\rho] = \tfrac{1}{2}\int\int \mathrm{d}^3r\,\mathrm{d}^3r'\,V(|\boldsymbol{r}-\boldsymbol{r}'|)\rho(\boldsymbol{r})\rho(\boldsymbol{r}'). \tag{6}$$

Equation (4) now takes, with the help of equations (5) and (6), the form

$$\Gamma^{-1}\frac{\partial\rho(\boldsymbol{r},t)}{\partial t} = k_BT\,\nabla_r^2\rho(\boldsymbol{r},t) + \nabla_r\rho(\boldsymbol{r},t)\cdot\int \mathrm{d}^3r'\,\nabla_r V(|\boldsymbol{r}-\boldsymbol{r}'|)\rho(\boldsymbol{r}',t) + \rho(\boldsymbol{r},t)\int \mathrm{d}^3r'\,\nabla_r^2 V(|\boldsymbol{r}-\boldsymbol{r}'|)\rho(\boldsymbol{r}',t) + \nabla_r\rho(\boldsymbol{r},t)\cdot\nabla_r V_{\mathrm{ext}}(\boldsymbol{r},t) + \rho(\boldsymbol{r},t)\,\nabla_r^2 V_{\mathrm{ext}}(\boldsymbol{r},t). \tag{7}$$

Given an initial density field $\rho(\boldsymbol{r}, t = 0)$ and a prescribed external potential $V_{\mathrm{ext}}(\boldsymbol{r}, t)$, equation (7) can be solved numerically to yield $\rho(\boldsymbol{r}, t)$. In this work we apply an ultrasoft Gaussian pair potential between the interacting particles that has been shown to describe the effective interaction between the centres of mass of polymer chains in athermal solvents [9, 14]:

$$V(r) = \epsilon\exp[-(r/\sigma)^2]. \tag{8}$$

We set $\epsilon = k_BT$, providing the energy unit for the problem, whereas σ, which corresponds to the gyration radius of the polymers, will be the unit of length henceforth. Accordingly, the natural timescale of the problem, providing the unit of time in this work, is the Brownian timescale $\tau_{\mathrm{B}} = \sigma^2/(\epsilon\Gamma)$. Equation (7) is solved iteratively using standard numerical techniques, and for a variety of time-dependent confining external potentials $V_{\mathrm{ext}}(\boldsymbol{r}, t)$ to be specified below.

BD simulations of equation (1) are also straightforward to carry out. The Langevin equations of motion including the external field are numerically solved using a finite time step $\Delta t = 0.003\,\tau_{\mathrm{B}}$ in all simulations, and the technique of Ermak [15, 16]. In order to obtain the time-dependent density $\rho(\boldsymbol{r}, t)$ we perform a large number N_{run} of independent runs, typically $N_{\mathrm{run}} = 5000$, and average the density profile over all configurations for a fixed time t.

We focus on external fields that correspond to a sudden change, i.e., $V_{\mathrm{ext}}(\boldsymbol{r}, t) = \Phi_1(\boldsymbol{r})\Theta(-t) + \Phi_2(\boldsymbol{r})\Theta(t)$. These force the system to relax from the equilibrium density $\rho_1(\boldsymbol{r}) = \rho(\boldsymbol{r}, t < 0)$, compatible with the external potential $\Phi_1(\boldsymbol{r})$, to the new equilibrium density $\rho_2(\boldsymbol{r}) = \rho(\boldsymbol{r}, t \to \infty)$, corresponding to the external potential $\Phi_2(\boldsymbol{r})$. Important questions related to such processes are those of what the typical relaxation time τ is for such a procedure and how the system crosses over from one equilibrium density to the other. We consider confinements of two kinds: spherical ones, $V_{\mathrm{ext}}(\boldsymbol{r}, t) = V_{\mathrm{ext}}(r, t)$, where $r = |\boldsymbol{r}|$; and planar ones between two walls perpendicular to the Cartesian z-direction, $V_{\mathrm{ext}}(\boldsymbol{r}, t) = V_{\mathrm{ext}}(z, t)$. In these cases we obtain $\rho(\boldsymbol{r}, t) = \rho(r, t)$ and $\rho(\boldsymbol{r}, t) = \rho(z, t)$, respectively, and the solution of equation (7) is greatly simplified since the integrals take the form of one-dimensional convolutions that can be evaluated very rapidly by the use of fast Fourier transform techniques.

Three different external confinements have been specifically investigated—two spherical ones:

$$V_{\mathrm{ext}}^{(1)}(r, t) = \Phi_0[(r/R_1)^2\Theta(-t) + (r/R_2)^2\Theta(t)], \tag{9}$$

$$V_{\mathrm{ext}}^{(2)}(r, t) = \Phi_0[(r/R_1)^{10}\Theta(-t) + (r/R_2)^{10}\Theta(t)]; \tag{10}$$

and one slab confinement:

$$V_{\mathrm{ext}}^{(3)}(z, t) = \Phi_0[(z/Z_1)^{10}\Theta(-t) + \phi(z/Z_2)^{10}\Theta(t)]. \tag{11}$$

The energy scale Φ_0 sets the strength of the confining potential and is fixed to $\Phi_0 = 10\,k_BT$ for all three confinements. The only difference between the external potential for times $t < 0$ and for $t > 0$ lies in the different length scales $R_2 \neq R_1$, for equations (9) and (10), and $Z_1 \neq Z_2$, for equation (11). For each confinement we consider two cases that give rise to two different dynamical processes: $R_1 < R_2$ ($Z_1 < Z_2$), enforcing an *expansion* of the system, and

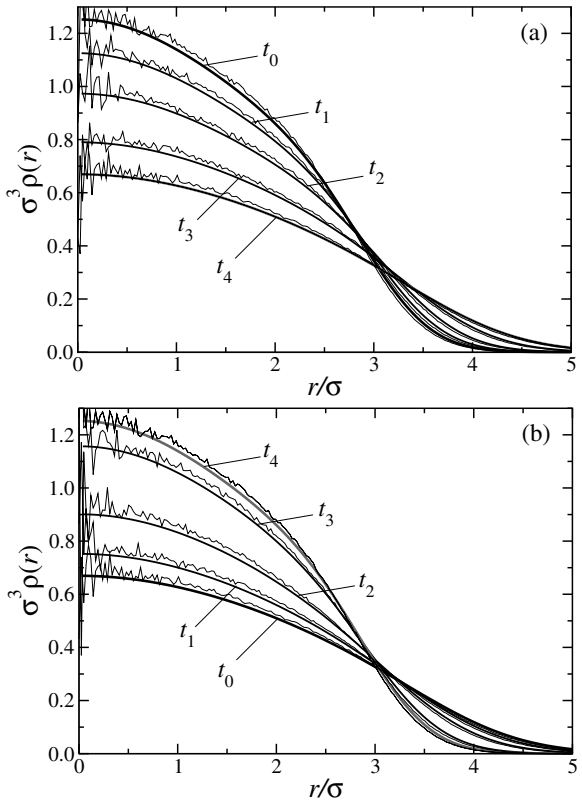

Figure 1. DDFT (solid curves) and BD (noisy curves) results for the time development of the radial density profiles $\rho(r)$ in the spherical confining potential $V_{\rm ext}^{(1)}(r,t)$ with (a) $R_1 = 4.0$ and $R_2 = 6.0$ and (b) $R_1 = 6.0$ and $R_2 = 4.0$. The profiles shown are for the times $t_0 = 0$, $t_1 = 0.06$, $t_2 = 0.18$, $t_3 = 0.54$ and $t_4 = 2.0$, all in $\tau_{\rm B}$-units. The last time is practically equivalent to $t = \infty$, since the system there has fully relaxed to equilibrium. In all figures, thick black curves denote the initial and thick grey ones the final static profile.

$R_1 > R_2$ ($Z_1 > Z_2$), bringing about a *compression* of the same. For the spherical confinements an additional parameter is the particle number $N = \int {\rm d}^3 r\, \rho(r,t)$ which is a conserved quantity, as is clear from equation (4) that has the form of a continuity equation. N enters the formalism through the normalization of the density field at $t = 0$. For both spherical confinements, the particle number is $N = 100$. In the slab confinement, equation (11), the conserved quantity is the density per unit area $\rho_0 = \int {\rm d}z\, \rho(z,t)$. We choose $\rho_0\sigma^2 = 10$. In all cases examined, the typical relaxation time was found to be of order $\tau_{\rm B}$; after typically $t = 2\ \tau_{\rm B}$, the system fully relaxes into the new equilibrium profile.

In figure 1 we show the results for the harmonic confining potential of equation (9). It can be seen that the theory reproduces the time evolution of the density profile, for both the expansion (figure 1(a)) and the compression (figure 1(b)) processes. An asymmetry of the two processes can already be discerned: the compression is not the 'time reverse' of the expansion and this effect will be much stronger in the examples to follow. Although the profiles of the system are very different from those of an ideal gas, i.e., effects of the interparticle interaction are present, the confining potential is smooth enough that the profiles are devoid of pronounced correlation peaks.

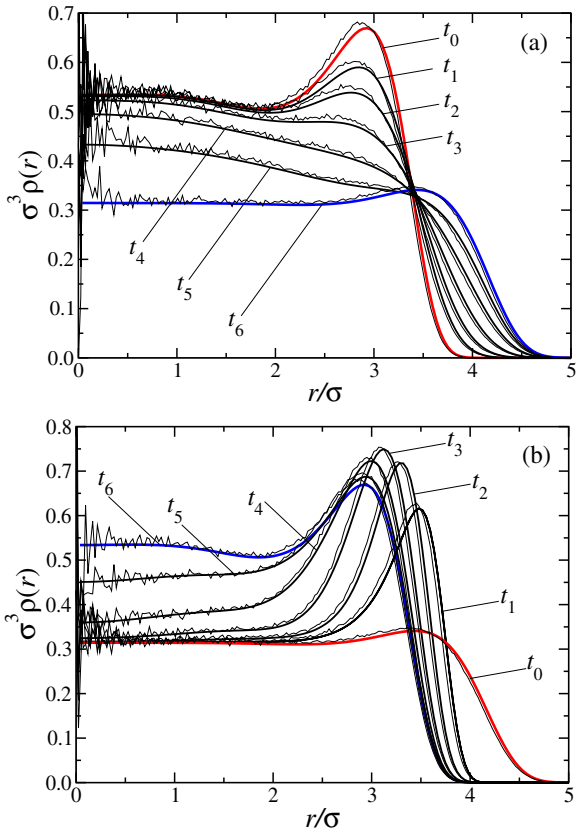

Figure 2. DDFT (solid curves) and BD (noisy curves) results for the time development of the radial density profiles $\rho(r)$ in the spherical confining potential $V_{\rm ext}^{(2)}(r, t)$ with (a) $R_1 = 4.0$ and $R_2 = 5.0$ and (b) $R_1 = 5.0$ and $R_2 = 4.0$. The profiles shown are for the times $t_0 = 0$, $t_1 = 0.03$, $t_2 = 0.06$, $t_3 = 0.12$, $t_4 = 0.24$, $t_5 = 0.48$ and $t_6 = 2.0$ (in units of $\tau_{\rm B}$).

The situation is different for the external potential of equation (10). Here, the power-law dependence is much steeper, so the Gaussian fluid develops correlation peaks close to the 'walls' of the confining field. The dynamical developments of the profiles for the expansion and compression processes are shown in figure 2. Here, the asymmetry between the expansion and the compression processes is evident. In the former case, seen in figure 2(a), the expansion of the confining potential leaves behind a density profile that has very strong density gradients close to the boundary of the initial confinement. Since the latter ceases to act at $t = 0$, this leaves at $t = 0^+$ instantaneously a region $R_1 < r < R_2$ that is devoid of particles but in which the new external potential is essentially zero. This leads to a collective diffusion of the particles towards the boundaries set by the new potential. Correspondingly, the high-density peaks decrease rapidly and leak outward. In the inner region, $r \approx 0$, of the profile, the dynamics is much slower and the relaxation to the final plateau there takes place at the end of the process, thereby causing the final development of the new, weaker correlation peaks close to the location of the boundary, $r \lesssim R_2$.

The compression process, depicted in figure 2(b), runs very differently. There, the initial 'closing' of the potential from R_1 to $R_2 < R_1$ leaves at $t = 0^+$ a region of high density at $R_1 < r < R_2$ that now finds itself within a strongly repulsive external field. There is an

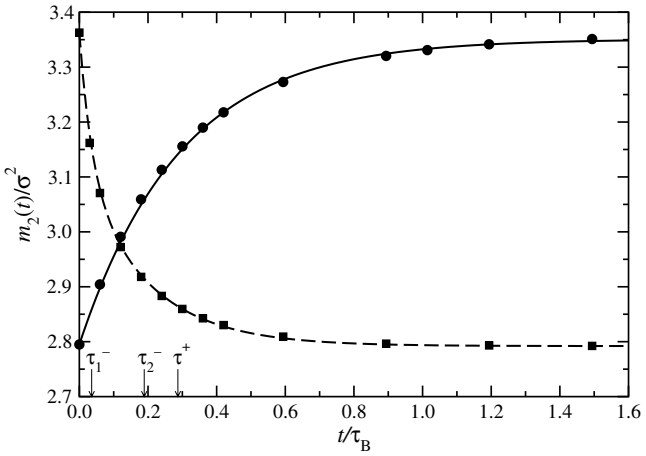

Figure 3. The second moment of the radial density profile, $m_2(t)$, defined in equation (12) plotted against the time t for the spherical confinement $V_{\rm ext}^{(2)}(r,t)$. Circles correspond to radii $R_1 = 4.0$ and $R_2 = 5.0$ (expansion) and squares show the resulting curve for the inverse process, $R_1 = 5.0$ and $R_2 = 4.0$ (compression). The curves are the analytical fits shown in the text. Solid curve: equation (13); long-dashed curve: equation (14). The arrows mark the characteristic timescales defined in these two equations.

extremely rapid shrinking there, accompanied by the development of very high correlation peaks that actually 'overshoot' in height with respect to the final equilibrium profile. Initially, the region in the centre of the sphere remains unaffected; only as the high peaks start diffusing does material flow toward the centre, and at the latest stage of the dynamics the profile at $r = 0$ reaches its new equilibrium value.

In order to quantify better this asymmetry and also extract characteristic timescales for the two dynamical processes, we consider the second moment of the density, $m_2(t)$, defined through

$$m_2(t) = \int \mathrm{d}^3 r\, r^2 \rho(r,t). \tag{12}$$

The quantity $m_2(t)$ is a quantitative measure of the spread of $\rho(r,t)$ around the centre of the external field and its time evolution is shown in figure 3. Let the superscript '+' denote the expansion and the superscript '−' the compression process. Obviously, $m_2^{\pm}(0) = m_2^{\mp}(\infty)$ holds. We notice that for both processes $m_2(t)$ is a monotonic function of t, but some interesting differences arise when one fits the two curves by analytic functions, shown as lines in figure 3. The expansion can be very accurately described by a single exponential:

$$m_2^+(t) = m_2^+(0) + [m_2^+(\infty) - m_2^+(0)][1 - \exp(-t/\tau^+)], \tag{13}$$

with the characteristic timescale $\tau^+ = 0.287\ \tau_{\rm B}$. However, a double-exponential fit is necessary to parametrize the compression process, namely

$$m_2^-(t) = m_2^-(\infty) + A^- \exp(-t/\tau_1^-) + [m_2^-(0) - m_2^-(\infty) - A^-] \exp(-t/\tau_2^-), \tag{14}$$

with the fit parameter $A^- = 0.240\ \sigma^{-2}$ and the *two* characteristic timescales $\tau_1^- = 0.036\ \tau_{\rm B}$ and $\tau_2^- = 0.189\ \tau_{\rm B}$. Since $\tau_{1,2}^- < \tau^+$, it follows that the compression process is at any rate faster than the expansion one. The occurrence of the two distinct timescales $\tau_1^- \ll \tau_2^-$ in the compression requires some explanation. The fast process that takes place at times $t \sim \tau_1^-$ corresponds to the abrupt shrinking of the profile in the wings of the distribution and is caused

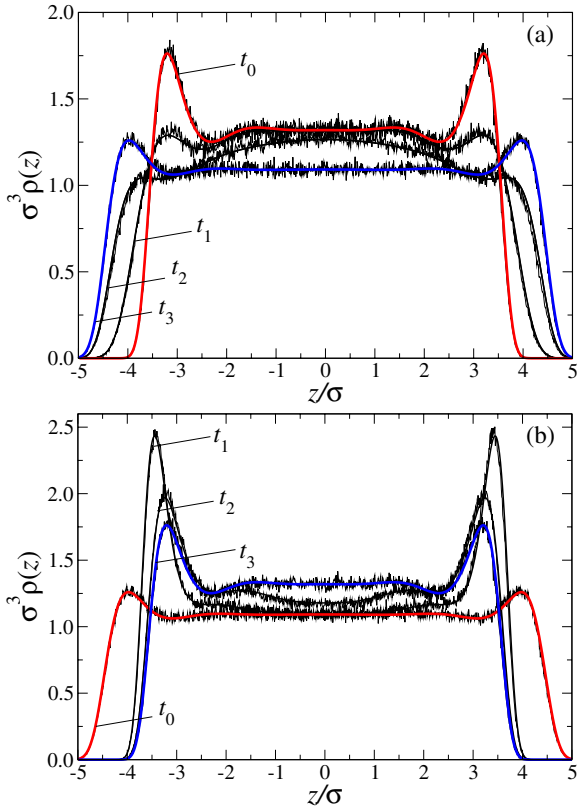

Figure 4. DDFT (solid curves) and BD (noisy curves) results for the time development of the linear density profile $\rho(z)$ in a slab confining potential $V_{\rm ext}^{(3)}(z,t)$ with (a) $Z_1 = 4.0$ and $Z_2 = 5.0$ and (b) $Z_1 = 5.0$ and $Z_2 = 4.0$. The profiles shown are for the times $t_0 = 0$, $t_1 = 0.06$, $t_2 = 0.24$ and $t_3 = 2.0$ (in units of $\tau_{\rm B}$).

exclusively by the 'closing' of the external field. This is the same mechanism as brings about the overshooting of the density peaks. Once this is over, diffusion within the now already confined system takes place and the second characteristic timescale, τ_2^-, is solely determined by the interaction potential $V(r)$ and the average particle density. In the expansion process, the first mechanism is absent. Thus a single timescale, τ^+, shows up, which is of intrinsic origin exclusively. Since stronger density gradients occur during the compression than during the expansion process, even the larger of the two timescales of the compression, τ_2^-, is smaller than τ^+. The denser the system, the faster the collective diffusion towards equilibrium.

Finally, we turn our attention to the slab confinement. The results from theory and simulation are shown in figure 4. Once more it can be seen that the DDFT offers an excellent description of the dynamics of the system. The same asymmetry between expansion and compression as was seen in the spherical confinement also shows up for the case of the slab, including the overshooting of the peaks during the compression process. In addition, the density profiles develop, during their evolution, secondary oscillations that are also very well reproduced by the theory.

In summary, we have demonstrated that the dynamical density functional theory of Marini Bettolo Marconi and Tarazona [4, 5], when supplemented by an accurate equilibrium density

functional, can provide an excellent description of out-of-equilibrium dynamics of colloidal systems at the Brownian timescale. The accuracy of the DDFT formalism has already been successfully tested for the system of one-dimensional hard rods [4], for which the exact density functional $F[\rho]$ is known. To the best of our knowledge, this is the first study of the validity of DDFT in three dimensions. As the phenomenology in 3D is much richer than that in 1D, including the possibility of phase transitions, many interesting paths to future applications open up.

Discussions with Andrew Archer, Bob Evans, Wolfgang Dietrich and Pedro Tarazona are gratefully acknowledged. This work was supported by the Deutsche Forschungsgemeinschaft through the SFB TR6.

References

[1] Evans R 1979 *Adv. Phys.* **28** 143
[2] Likos C N 2001 *Phys. Rep.* **348** 267
[3] Dhont J K G 1996 *An Introduction to Dynamics of Colloids* (Amsterdam: Elsevier)
[4] Marini Bettolo Marconi U and Tarazona P 1999 *J. Chem. Phys.* **110** 8032
[5] Marini Bettolo Marconi U and Tarazona P 2000 *J. Phys.: Condens. Matter* **12** A413
[6] Dietrich W, Frisch H L and Majhofer A 1990 *Z. Phys.* B **78** 317
[7] Lang A, Likos C N, Watzlawek M and Löwen H 2000 *J. Phys.: Condens. Matter* **12** 5087
[8] Likos C N, Lang A, Watzlawek M and Löwen H 2001 *Phys. Rev.* E **63** 031206
[9] Louis A A, Bolhuis P G and Hansen J-P 2000 *Phys. Rev.* E **62** 7961
[10] Archer A J and Evans R 2001 *Phys. Rev.* E **64** 041501
[11] Archer A J and Evans R 2002 *J. Phys.: Condens. Matter* **14** 1131
[12] Archer A J, Likos C N and Evans R 2002 *J. Phys.: Condens. Matter* **14** 12031
[13] Archer A J, Evans R and Roth R 2002 *Europhys. Lett.* **59** 526
[14] Louis A A, Bolhuis P G, Hansen J-P and Meijer E J 2000 *Phys. Rev. Lett.* **85** 2522
[15] Allen M P and Tildesley T J 1989 *Computer Simulation of Liquids* (Oxford: Clarendon)
[16] Ermak D L 1975 *J. Chem. Phys.* **62** 4189